frontiers in Neurology

ORIGINAL RESEARCH
published: 07 April 2021
doi: 10.3389/fneur.2021.663722

Vestibular Organ and Cochlear Implantation–A Synchrotron and Micro-CT Study

Hao Li[1], *Nadine Schart-Moren*[1,2], *Gunesh Rajan*[3,4], *Jeremy Shaw*[5], *Seyed Alireza Rohani*[6], *Francesca Atturo*[7], *Hanif M. Ladak*[6,8†], *Helge Rask-Andersen*[1*†] *and Sumit Agrawal*[6,8†]

[1] *Department of Surgical Sciences, Otorhinolaryngology and Head and Neck Surgery, Uppsala University, Uppsala, Sweden,* [2] *Section of Otolaryngology, Head and Neck Surgery, Uppsala University Hospital, Uppsala, Sweden,* [3] *Department of Otolaryngology, Head & Neck Surgery, Luzerner Kantonsspital, Lucerne, Switzerland,* [4] *Department of Otolaryngology, Head & Neck Surgery, Division of Surgery, Medical School, University of Western Australia, Perth, WA, Australia,* [5] *Centre for Microscopy, Characterization and Analysis, Perth, WA, Australia,* [6] *Department of Otolaryngology-Head and Neck Surgery, Western University, London, ON, Canada,* [7] *Department of Otolaryngology, University of Sapienza, Rome, Italy,* [8] *Department of Medical Biophysics and Department of Electrical and Computer Engineering, Western University, London, ON, Canada*

Background: Reports vary on the incidence of vestibular dysfunction and dizziness in patients following cochlear implantation (CI). Disequilibrium may be caused by surgery at the cochlear base, leading to functional disturbances of the vestibular receptors and endolymphatic duct system (EDS) which are located nearby. Here, we analyzed the three-dimensional (3D) anatomy of this region, aiming to optimize surgical approaches to limit damage to the vestibular organ.

Material and Methods: A total of 22 fresh-frozen human temporal bones underwent synchrotron radiation phase-contrast imaging (SR-PCI). One temporal bone underwent micro-computed tomography (micro-CT) after fixation and staining with Lugol's iodine solution (I_2KI) to increase tissue contrast. We used volume-rendering software to create 3D reconstructions and tissue segmentation that allowed precise assessment of anatomical relationships and topography. Macerated human ears belonging to the Uppsala collection were also used. Drilling and insertion of CI electrodes was performed with metric analyses of different trajectories.

Results and Conclusions: SR-PCI and micro-CT imaging demonstrated the complex 3D anatomy of the basal region of the human cochlea, vestibular apparatus, and EDS. Drilling of a cochleostomy may disturb vestibular organ function by injuring the endolymphatic space and disrupting fluid barriers. The saccule is at particular risk due to its proximity to the surgical area and may explain immediate and long-term post-operative vertigo. Round window insertion may be less traumatic to the inner ear, however it may affect the vestibular receptors.

Keywords: human, synchrotron, micro-CT, vestibular organ, cochlear implant

OPEN ACCESS

Edited by:
Louis Murray Hofmeyr,
Stellenbosch University, South Africa

Reviewed by:
Wilhelm Wimmer,
University of Bern, Switzerland
Stefan Weber,
University of Bern, Switzerland

***Correspondence:**
Helge Rask-Andersen
helge.rask-andersen@surgsci.uu.se
orcid.org/0000-0002-2552-5001

†These authors share senior authorship

Specialty section:
This article was submitted to Neuro-Otology, a section of the journal Frontiers in Neurology

Received: *03 February 2021*
Accepted: *15 March 2021*
Published: *07 April 2021*

Citation:
Li H, Schart-Moren N, Rajan G, Shaw J, Rohani SA, Atturo F, Ladak HM, Rask-Andersen H and Agrawal S (2021) Vestibular Organ and Cochlear Implantation–A Synchrotron and Micro-CT Study. Front. Neurol. 12:663722. doi: 10.3389/fneur.2021.663722

INTRODUCTION

There are various reports on the incidence of vestibular dysfunction and vertigo following cochlear implantation (CI) in adults and children. Although CI is considered to be safe, the traumatic action of electrode insertion into the cochlea risks impairing vestibular function. Seriously incapacitating vertigo is rare, and there is usually complete resolution (1). Different factors have been ascribed

as possible causes, such as labyrinthine status before CI surgery or concurrent inner ear disease. Older patients and patients with preoperative dizziness may be more prone to vestibular injury, and this may occasionally be associated with tinnitus and fluctuating hearing loss (2–5). Dizziness may be experienced directly after surgery or with delayed onset (6). In some instances, endolymphatic hydrops (EH) may be suspected (7). Therefore, vestibular impairment can be influenced by surgical impact, patient age, and cause of deafness.

The human ear contains five end-organs, each of which can be affected by surgery at the cochlear base or by electrode insertion itself. Postmortem histopathological studies of the temporal bones of CI recipients have reported significant structural changes in end-organs, including the saccule, the utricle, and the semicircular canals (8, 9). Injury of cochlear and vestibular tissue may lead to the mixing of fluids and the alteration of otolith membranes and receptor cells. CI may damage the lateral cochlear wall disturbing endolymph homeostasis leading to cochlear hydrops. CI may also obstruct endolymph flow between the cochlea and the saccule by blocking the reunion duct (RD) or cochlear duct causing cochlear hydrops and collapse of the saccule (9). Long-term changes may occur from inflammation, fibrosis, and ossification (8). There is a particular risk of damage to the saccule, which is located in the spherical recess close to the base of the cochlea and round window (RW). Moreover, the main cochlear vein is located in the floor of the scala tympani (ST) near the final position of the CI electrode.

Non-invasive, high-resolution synchrotron radiation and 3D imaging of temporal bone specimens have earlier been performed (10). To improve soft tissue contrast, chemical staining was also introduced to visualize the hearing organ and nerve elements using absorption based synchrotron imaging (11, 12). This necessitates opening of the windows of the inner ear with risk for artifact generation. In lieu of staining, synchrotron radiation phase-contrast imaging (SR-PCI) can be used to increase visualization of soft tissues. This technique exploits x-ray intensity variations to produce edge contrast thereby improving soft tissue visualization. At the same time, SR-PCI conserves visualization of bone while avoiding the artifacts introduced with staining, sectioning, and decalcification used in histopathology (13–15). Elfarnawany et al. first performed SR-PCI on intact human cochleae to obtain 3D reconstructions of cochlear soft tissues (16). The high-resolution scans obtained through this technique were capable of revealing cytoarchitecture similar to histology (17, 18). Subsequent groups have applied the SR-PCI technique to other parts of the temporal bone, including the middle ear and ossicles (19, 20). Recently, Anschuetz et al. demonstrated synchrotron radiation imaging of the human auditory ossicles at the sub-micron level (21).

The present study aimed to three-dimensionally analyze the intricate anatomy of the surgical region to optimize atraumatic approaches in CI to limit the surgical impact on the vestibular apparatus and associated neural pathways. A total of 22 fresh human temporal bones underwent SR-PCI and one fresh bone underwent micro-computed tomography (micro-CT) after fixation and staining with Lugol's iodine solution (I_2KI) to increase tissue contrast. In addition, we analyzed the archival temporal bone collection in Uppsala described in earlier investigations (22, 23). Different cochleostomies (COs) were made with metric analyses. Volume-rendering software was then used to create three dimensional (3D) reconstructions allowing tissue segmentation and detailed assessment of anatomical relationships, metric analyses, and topography. It was found that the RW surgical approach may be preferred to limit the risk for vestibular dysfunction and vertigo after CI, assuming there are no anatomical restrictions preventing this approach.

MATERIALS AND METHODS

Ethical Statements

Human Temporal Bones

Twenty-two adult human cadaveric cochleae were used in this study. Specimens were obtained with permission from the body bequeathal program at Western University, London, Ontario, Canada, in accordance with the Anatomy Act of Ontario and Western's Committee for Cadaveric Use in Research (approval no. 06092020). Ethics approval for the micro-CT project was obtained from the University of Western Australia (UWA, RA/4/1/5210), and the human temporal bones were provided by the Department of Anatomy at UWA.

The adult cadaveric temporal bones were fresh-frozen and then fixed in 3.7% formaldehyde and 1% glutaraldehyde in phosphate buffer for 5 days. The bones were thawed and cut to a sample (40 mm diameter, 60 mm length) from each temporal bone. All samples were cut from the middle ear toward the inner ear. The tissue was rinsed and dehydrated in a graded ethanol series. No staining, sectioning, or decalcification was performed on the specimens.

SR-PCI and Imaging Technique

The SR-PCI technique used in the present investigation was recently described by Elfarnawany et al. (16) and Koch et al. (13). Each sample was scanned using SR-PCI combined with CT at the Bio-Medical Imaging and Therapy (BMIT) 05ID-2 beamline at the Canadian Light Source, Inc. (CLSI) in Saskatoon, SK, Canada. The imaging field of view was set to 4,000 × 950 pixels corresponding to 36.0 × 8.6 mm, and 3,000 projections over a 180° rotation were acquired per CT scan. CT reconstruction was performed, and the 3D image volume had an isotropic voxel size of 9 μm. The acquisition time to capture all projections per view was ∼30 min. For 3D segmentations of the cochlear anatomy, structures were traced and color-labeled manually on each SR-PCI CT slice (approximately 1,400 slices per sample).

Abbreviations: ACO, Anterior cochleostomy; AICO, Anterior-inferior cochleostomy; BM, Basilar membrane; CA, Cochlear aqueduct; CI, Cochlear implantation; CO, Cochleostomy; Dice-CT, Diffusible iodine-based contrast-enhanced computed tomography; EH, Endolymphatic hydrops; IAC, Internal acoustic canal; ICO, Inferior cochleostomy; ICV, Inferior cochlear vein; I_2KI, Lugol's iodine solution; LSSC, Lateral semicircular canal; LVAS, Large vestibular aqueduct syndrome; Micro-CT, Micro-computed tomography; OSL, Osseous spiral lamina; OW, Oval window; PSSC, Posterior semicircular canal; RD, Reunion duct; RM, Reissner's membrane; RW, Round window; SG, Spiral ganglion; SL, Spiral ligament; SR-PCI, Synchrotron radiation phase-contrast imaging; ST, Scala tympani; VEMPS, Vestibular-evoked myogenic potentials; vHIT, Video head impulse test; VOR, Vestibule-ocular reflex.

The open source medical imaging software, 3D Slicer version 4.10 (24), was used to create detailed 3D representations of the basilar membrane (BM), spiral ganglion (SG), and connective dendrites between these structures, which allowed for accurate delineation when compared with traditional two-dimensional (2D) slices. Measurements were made in 22 temporal bones by two independent observers. Distances from the utricle macula, posterior semicircular canal ampulla, saccule macula, and saccule membrane to the middle of the RW were assessed.

Micro-CT

Micro-CT was used to analyze the 3D anatomy of the nerves in the internal acoustic meatus. We used a diffusible iodine-based technique to enhance contrast of soft tissues for diffusible iodine-based contrast-enhanced computed tomography (dice-CT) (25). Increased time penetration of Lugol's iodine (aqueous I_2KI, 1% I_2, 2% KI) offers possibilities to visualize between and within soft tissue structures (25). The temporal bone was fixed in a modified Karnovsky's fixative solution of 2.5% glutaraldehyde, 1% paraformaldehyde, 4% sucrose, and 1% dimethyl sulfoxide in 0.13 M of Sorensen's phosphate buffer. Soft tissue contrast was achieved by staining the sample for 14 days, as described by Culling et al. (26). X-ray micro-CT was conducted using a Versa 520 XRM (Zeiss, Pleasanton, CA, USA) running Scout and Scan software (v11.1.5707.17179). Scans were conducted at a voltage of 80 kV and 87 μA, using the LE4 filter under 0.4× optical magnification and a camera binning of 2. Source and detector positions were adjusted to deliver an isotropic voxel size of 23 μm. A total of 2,501 projections were collected over 360°, each with an exposure time of 1 s. Raw projection data were reconstructed using XM Reconstructor software (v10.7.3679.13921; Zeiss) following a standard center shift and beam hardening (0.1) correction. The standard 0.7 kernel size recon filter setting was also used.

Uppsala Temporal Bone Collection

We used the archival human temporal bones from autopsies and 324 plastic and silicone molds described in earlier publications (22, 23). The collection was established during the 1970s and 1980s at the Department of Diagnostic Radiology and Otolaryngology at Uppsala University Hospital (27, 28). All bones and molds underwent micro-CT as described earlier (23). The topographic anatomy of the "hook" region with relationships between the oval window (OW), RW, osseous spiral lamina (OSL), and spiral ligament (SL) were examined and photographed as described earlier by Atturo et al. (29). Different sized cochleae were analyzed and conventional anterior (ACOs), antero-inferior (AICOs), and inferior COs were made, including the enlarged RW approach (30, 31). The proximity of various COs to the vestibular organ was studied, both from "inside" and "outside" the labyrinth.

RESULTS

SR-PCI and micro-CT with contrast enhancement reproduced both the soft and bony tissue of the human cadaver labyrinth. A notable 3D reproduction of the membranous labyrinth in a left human temporal bone is shown in **Figure 1**. The cochlear and

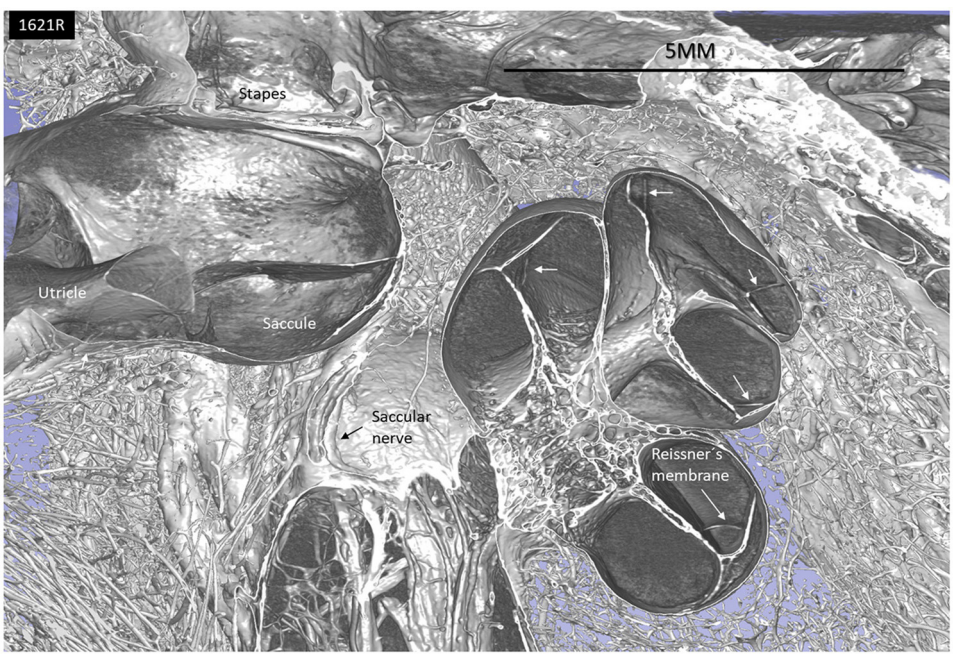

FIGURE 1 | SR-PCI and 3D reconstruction of a left human inner ear (superior view) using 3D slicer (version 4.10; www.slicer.org). The cochlea, utricle, saccule, and saccular nerve are seen with cranial nerves in the fundus of the IAC.

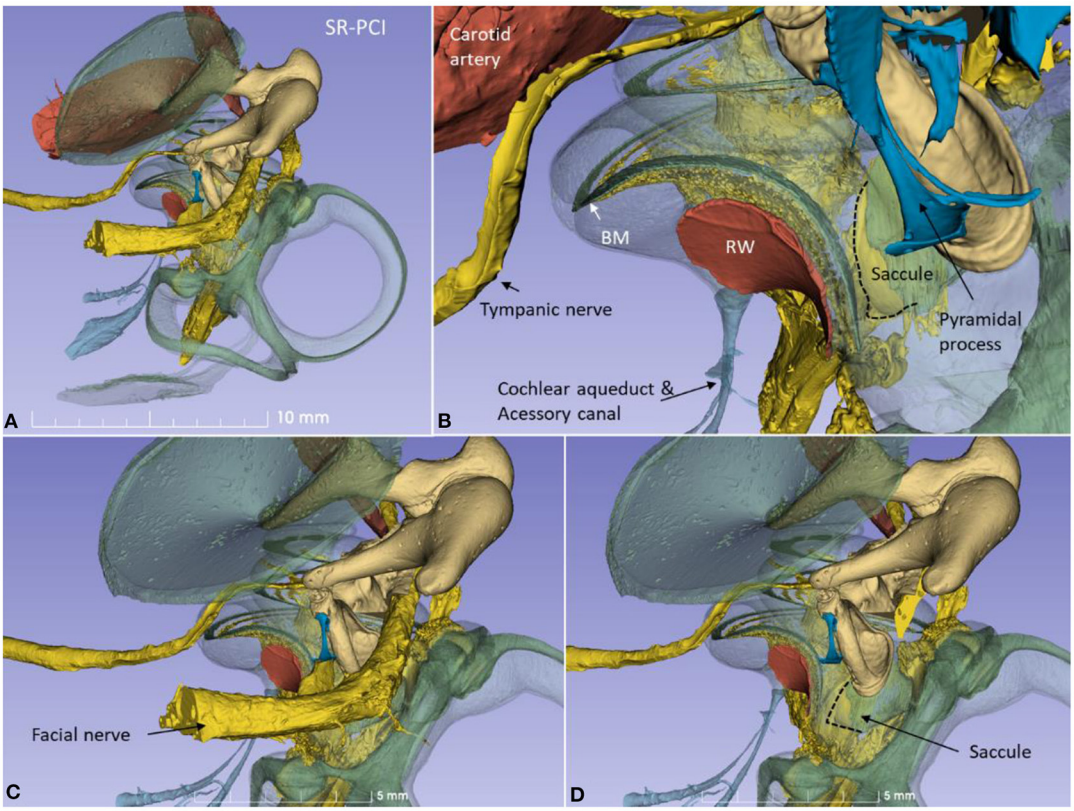

FIGURE 2 | (A) SR-PCI 3D modeling of a left human temporal bone with a surgical view through the facial recess. **(B)** The relationship between the RW and the saccule is seen. The cochlear aqueduct (CA) and a second accessory canal are seen. **(C,D)** show the facial recess anatomy with **(C)** and without **(D)** the facial nerve.

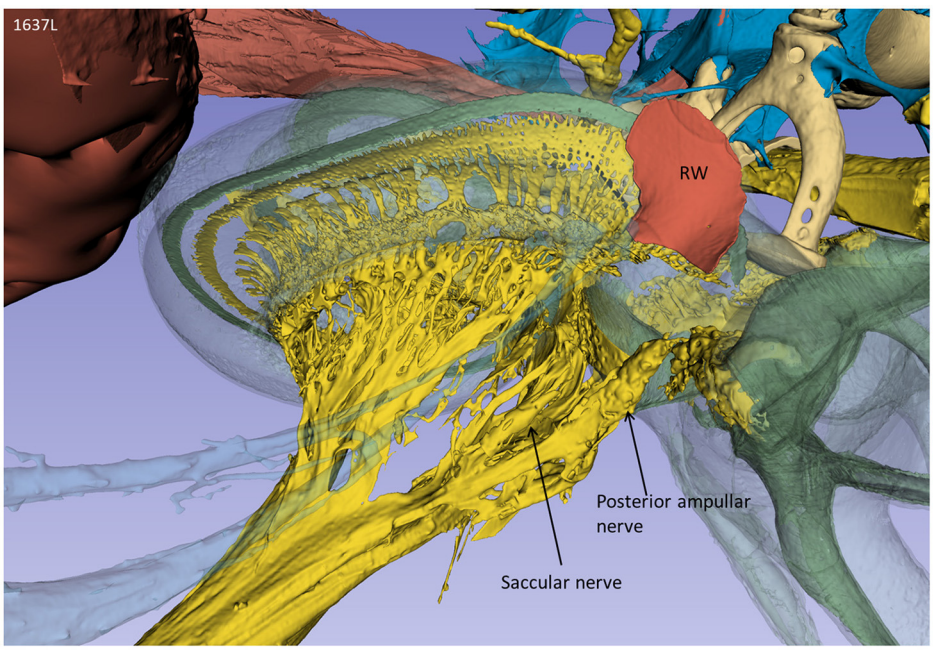

FIGURE 3 | A posterior-inferior view of the specimen shown in **Figure 2**. The relationships between the RW and the posterior ampulla and saccular nerves are shown. The distance between the middle of the RW and the middle part of the posterior ampulla was 2.6 mm.

vestibular nerves and their branches could be followed from the internal acoustic canal (IAC) to the peripheral organs.

The 3D modeling shows the surgical anatomy through the facial recess (**Figure 2**). The anatomical details of the cochlear base are visualized together with the saccule and utricle. Removal of the facial nerve demonstrates the close relationship between the cochlea and the saccule.

From an inferior angle, the relationship between the RW and the saccular and posterior ampulla nerves is shown (**Figure 3**).

Lateral sectioning at the cochlear base of a left ear demonstrates the relationship between the saccule and utricle and the ST in more detail (**Figure 4**). Electrode insertion near the posterior corner of the RW and at an acute angle may jeopardize the OSL with consequences of entering the vestibule. The RD lies on the superior edge of the SL and connects the scala media and saccule. The RD is challenged if the bony lamina is perforated. The mean distance between the mid-portion of the RW and the saccule was 2.66 mm ($SD = 0.35$ mm) and between the RW and the saccule macula was 3.21 mm ($SD = 0.29$ mm). The mean distance between the RW and the utricle macula was 3.79 mm ($SD = 0.32$ mm) (**Supplementary Table 1**).

The saccular wall consists of both a thick and a thin part. The two parts are separated by a thickening in the membrane. The thin part faces the middle ear, while the thick part reinforces the saccule against the spherical recess. The thin part was difficult to reproduce three-dimensionally and gave the impression of an imperfection in the wall.

The macerated human ears revealed extensive anatomic variations of the basal or "hook" region of the cochlea. Drilling and insertion of a CI electrode via an anterior or anterior-inferior CO invariably damaged cochlear structures. Membrane rupture may lead to a mixture of fluids, and bone dust potentially contaminates the vestibule with risk for damage to the vestibular receptors. The soft tissue suspending the BM along the rim of the RW varied among individuals, and even an inferiorly located CO occasionally damaged cochlear tissues. A larger distance between the OW and RW seemed to diminish the risk for mechanical trauma to the SL at inferior CO drilling. Smaller cochleae increased the risk of injuring the SL by leading to a direct trajectory to the saccule. A RW inserted electrode is visualized in **Figure 5**, from "inside" the labyrinth. Distances from the utricle macula, saccule macula, and saccule membrane to the middle of the RW were measured in all 22 temporal bones and are shown in a box plot. The distances from different COs to the utricular and saccular macular nerve foramina were also assessed (**Figures 6**, **7**).

A virtual CI surgery using the RW approach in a 3D reconstructed human temporal bone from a micro-CT is demonstrated in **Figures 8**, **9**. The position of the saccule is seen after the bony capsule was made transparent (**Figures 8A,B**). The

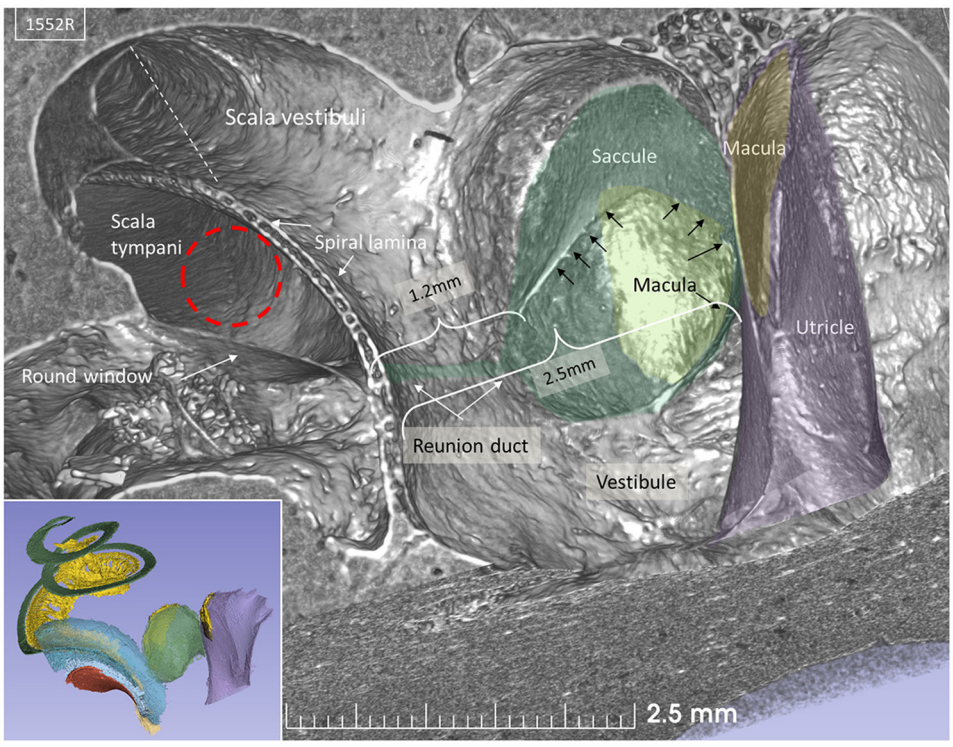

FIGURE 4 | SR-PCI section at the level of the RW and vestibule (lateral view). The RW and the position of a virtual electrode (dashed red line) are shown. The saccule lies in the spherical recess in the medial bony wall of the vestibule. It consists of a thicker and thinner part limited by thicker bands (arrows). The macula is stained yellow. The position of the RD is shown. Inset shows the modeled 3D anatomy with the saccule, RW (red), and spiral ligament of the cochlear base (blue). The broken line represents Reissner's membrane.

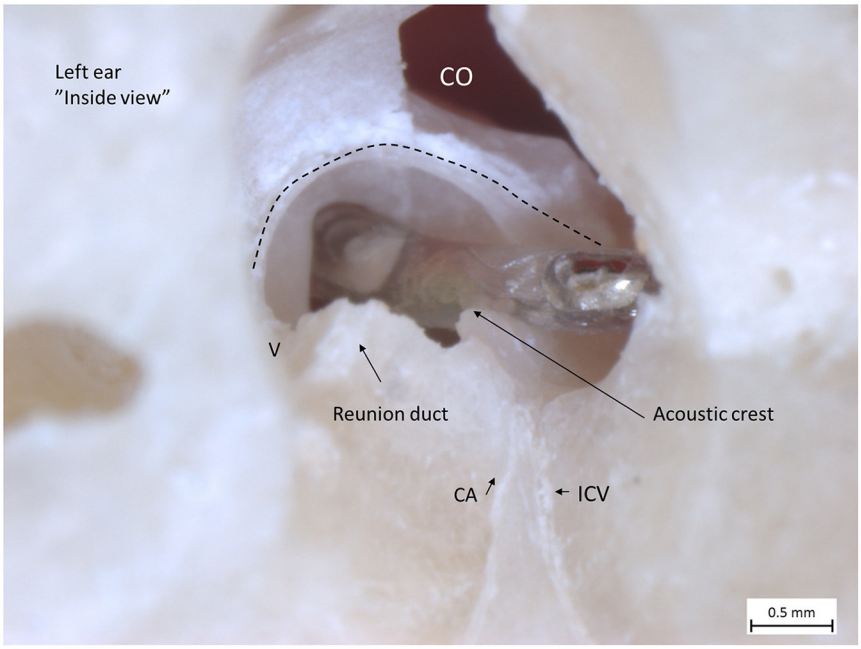

FIGURE 5 | Left human micro-dissected temporal bone (taken from the temporal bone collection of Uppsala Museum) shows the RW and acoustic crest from "inside" the labyrinth. The OSL was resected, with the secondary lamina partially preserved along the rim of the RW. The broken line shows the attachment of the BM around the RW. The electrode was inserted via the RW. It rides upon the acoustic crest before reaching the ST. An anterior CO was drilled. The CA and the inferior cochlear vein (ICV) channels were dissected as well as the RD.

lateral wall of the saccule is visualized through the OW, reaching cranially to the floor of the utricle. The inferior cochlear and saccular veins in the floor of the ST were found to be at low risk for damage.

DISCUSSION

To minimize damage during CI, it is important that the electrode is retained within the ST and that the integrity of the endolymph space is maintained. The surgical area at RW insertion is located ∼2.7 mm from the rim of the saccule membrane. At AICO and ACO, this distance is longer, but the risk for breaking the endolymph barrier is higher. Synchrotron imaging shows that the saccule wall consists of a thin and a thick portion. The thick portion lies near the bony margins of the spherical recess, and the thin portion faces the middle ear. The latter shows extreme fragility and may protect saccular receptors from high-energy stapes vibrations (32). This portion may be damaged or ruptured even by forceful mechanical pressure changes such as the "cork effect" at stapes removal. Entering the vestibular scala during cochleostomy increases the risk of bone dust entering the vestibule, which may lead to acute pro-inflammatory reactions and contribute to symptom manifestations. Moreover, the vibration produced by the milling process may cause statoconia dislocation and consequent vertigo. It may even explain benign positional vertigo, transient dizziness (33), and EH caused by dislocated saccular statoconia in the RD (34) (**Figure 10**). Therefore, direct drilling on the cochlear capsule should probably be kept to a minimum.

There are other explanations for acute or persistent dizziness following CI surgery, such as fistulae in patients with large vestibular aqueduct syndrome (LVAS) (35) or EH (7, 36). The saccular receptors seem particularly vulnerable, reflected by changes in vestibular-evoked myogenic potentials (VEMPs) (37). Alterations such as new bone formation, vestibular fibrosis, saccule membrane distortion, and sub-epithelial thickening were described in studies where the CO technique was mostly performed (8). The authors suggested that the saccule is at greater risk for damage than the utricle or semicircular canals. According to Todt et al. (38), CO may degrade saccular function demonstrated by affected VEMP, and this was correlated with persistent dizziness. Similar results were noted by Jin et al. (39) studying 12 children undergoing CI and by Meli et al. in adults showing lack or reduction of VEMP responses (40). Licamelli et al. (41) found a majority of patients had vestibular impairment with altered saccular function indicated by VEMP as well as reduced vestibule-ocular reflex (VOR) gain. Our 3D study revealed the small distance between the most proximal region of the RW and the saccule (**Figure 11**), which may suggest that this region of the RW should be avoided during surgery. In some children with inner ear dysplasia, VEMP responses were also observed at electrical stimulation, suggesting that the vestibular nerve may be stimulated (39). This may be explained by the posterior ampulla and nerve positioned near the RW (**Figure 11**, **Supplementary Tables 1, 2**).

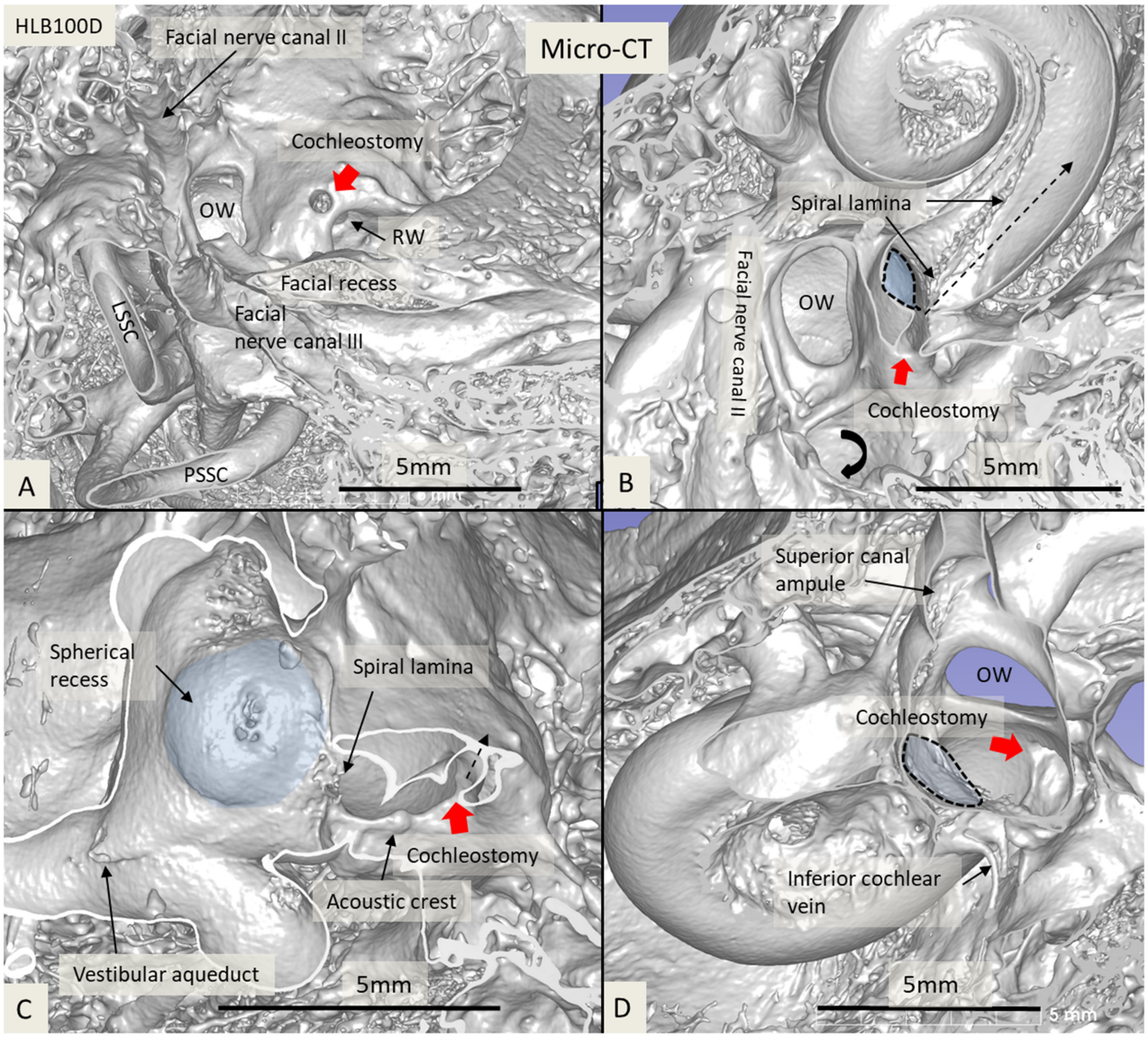

FIGURE 6 | Micro-CT and 3D reconstruction of a macerated human temporal bone (right ear). An anterior CO was made (red arrow), and its relation to the spherical recess (blue) and saccule was studied. **(A)** Surgical view shows the CO and the RW. **(B)** Lateral cropping demonstrates the entrance canal of the CO and its relation to the spherical recess. The bold arrow shows the tympanic sinus. **(C)** Medial cropping shows the spherical recess (blue) with bony foramina of the saccular nerve. The broken arrow shows the direction of the scala tympani. **(D)** Medial view shows CO and spherical recess (dashed line). OW, oval window; RW, round window; LSSC, lateral semicircular canal; PSSC, posterior semicircular canal.

Optimal preservation of residual hearing requires a more atraumatic CI surgery which can be expected to diminish injury to the vestibular organ as well. However, there are indications of some damage to the vestibular receptors of the otolith organs and semicircular canals even when using soft surgery techniques (42). Insertion speed was found to influence hearing preservation and vestibular function. A slow electrode insertion speed seemed to facilitate complete insertion, and improved preservation of residual hearing and vestibular function after CI (43). Fortunately, patients with vertigo usually undergo central vestibular compensation and recover with little or no postural deficit (40). However, it has not been determined whether the surgical approach and design of electrodes influence the prevalence of vestibular problems. Synchrotron 3D analyses show that the RW approach may be less damaging to the inner ear compared with CO (15, 23), which is in accordance with the vestibular results obtained by Todt et al. (38). Batuecas-Caletrio et al. (44) found the RW approach safer and less traumatic than CO. However, no correlation between the surgical approach and occurrence of postoperative vertigo was found by Veroul et al. (45) or by Nassif et al. (46), who investigated children. Rah et al. (7) found that the RW approach resulted in less postoperative

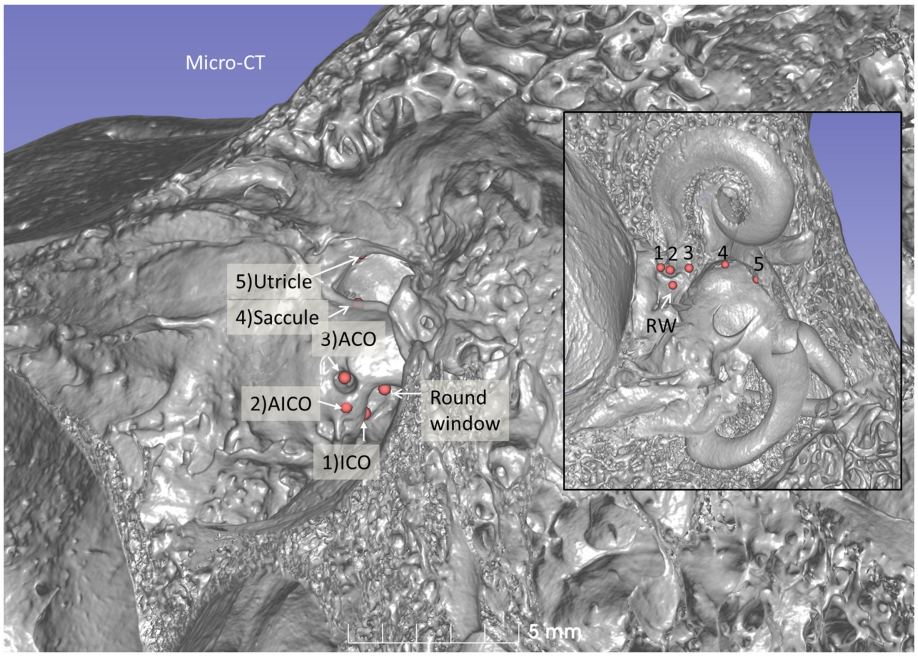

FIGURE 7 | Micro-CT 3D reconstruction of a left human temporal bone (lateral view). An ACO (3) was made, and the distances to the saccular (4) and utricular (5) nerve foramina can be assessed (inset). Virtual AICO (2) and ICO (1) are shown with fiducials.

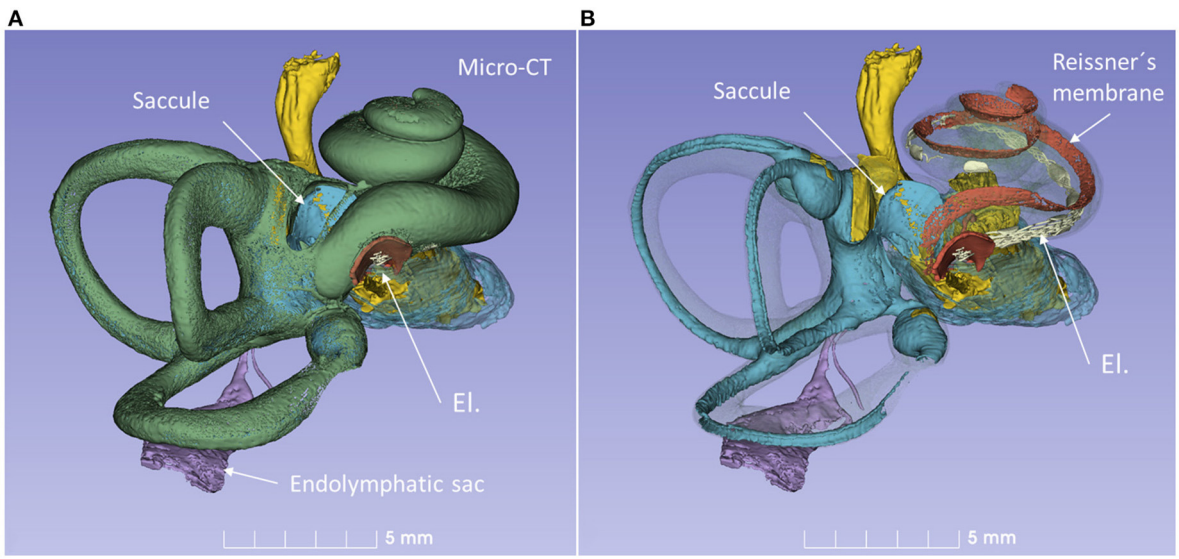

FIGURE 8 | 3D model of a right human temporal bone from micro-CT. Increased penetration time of aqueous I_2KI improved visualization of soft tissue structures. The cochlea was virtually implanted with an electrode (El) through the RW. **(A)** With bone capsule. **(B)** Bone capsule was made transparent to visualize the inner ear soft tissues.

dizziness, but this was not statistically significant due to the small numbers of RW insertions. Hänsel et al. (47) performed a meta-analysis and showed a low incidence of postoperative vertigo, but it was slightly higher in the CO group compared with the RW group. A CO closer to the RW was said to reduce the BM penetrations (48). In our opinion, it is difficult to foresee the extent of the damage that may occur from using the CO technique even if drilling is performed far inferiorly near the acoustic crest at the RW (22, 49). It may appear possible to directly enter the ST, however due to the surgical angle and curved outline of the SL, it may not actually be the case. Nonetheless, there may be anatomical limitations that necessitate a CO, such as facial recess exposure, cochlear malformations, and angles reducing the visibility of the RW.

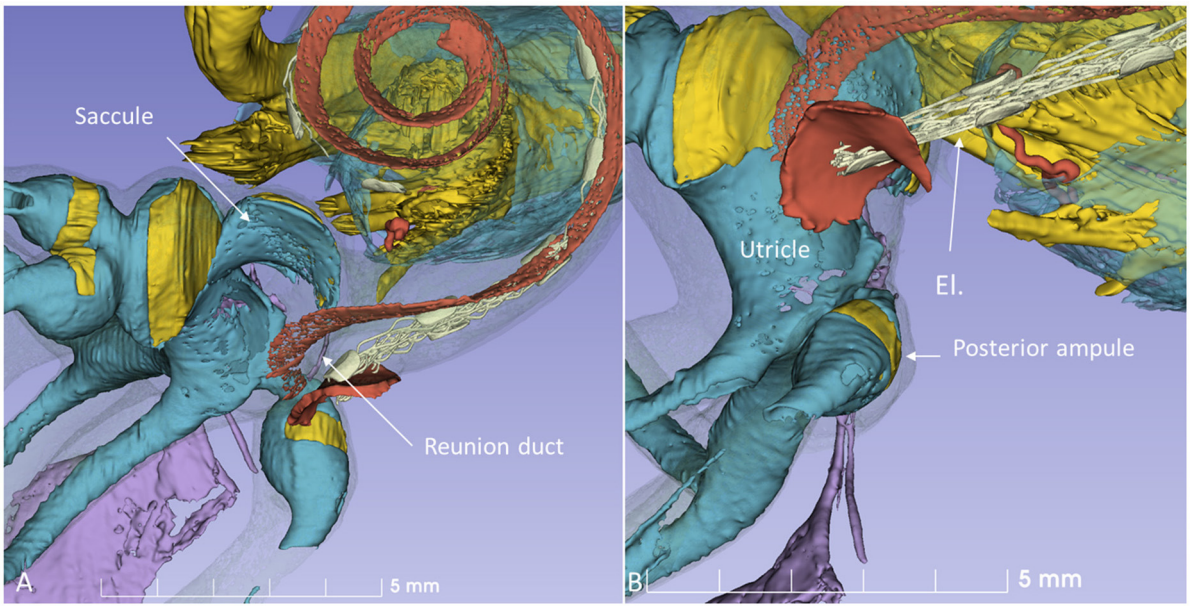

FIGURE 9 | 3D model in **Figure 8** is shown at higher magnification. **(A)** The modeled RD is seen. **(B)** The posterior ampule and its relation to the RW can be seen. El, cochlear implant electrode.

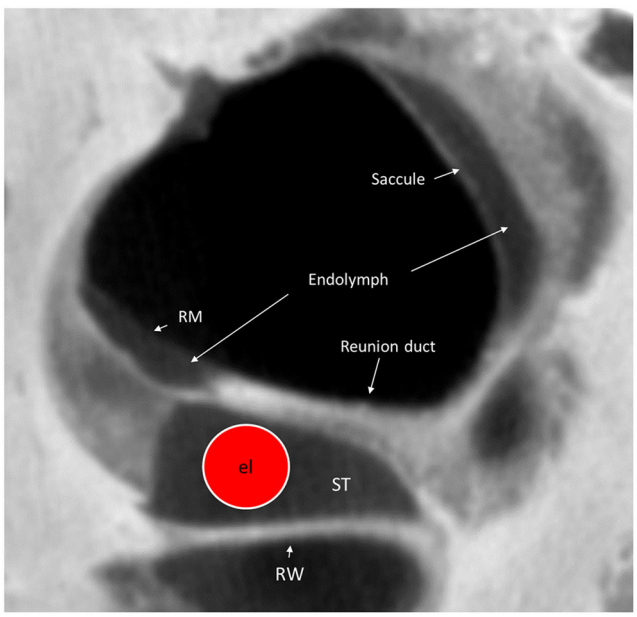

FIGURE 10 | Micro-CT cross-section of the cochlear base at the RW. A virtual CI electrode (el) is placed in the scala tympani. The RD can hardly be seen on the superior surface of the OSL. RM, Reissner's membrane; ST, scala tympani; RW, Round window.

CI can also influence horizontal semicircular canal function, and the video head impulse test (vHIT) and caloric test have been recommended for a complete vestibular analysis (50). RW surgery may change canal and otolith organ function, as shown by Dagkiran et al. (51). They found that the posterior and superior semicircular canal functions were more affected than the lateral canal, recommending the use of a test battery capable of evaluating all five vestibular end-organs pre- and postoperatively. In a recent study in patients undergoing unilateral or bilateral CI, there was no significant impairment of lateral semicircular canal function as demonstrated by high-frequency VOR and vHIT compared with normal hearing individuals in the long term (46, 52). According to Nassif et al. (46), vHIT results suggest there is little impairment of LSSC function compared with normal hearing children (52). From an anatomical standpoint, a functional deterioration of the lateral and horizontal canals is likely to be caused by an indirect trauma caused by perilymph drain or contamination at surgery. Interestingly, SR-PCI revealed that the vestibular membrane apparatus is anchored by several gracile tissue pillars reaching the interior surface of the bony labyrinth. A massive drain of perilymph could rupture this fine network and lead to organ displacement and vestibular dysfunction. These findings may further point to the importance of a slow electrode insertion to minimize perilymph displacement and allow adaptation inside the scala and vestibule to reduce trauma.

Today, most congenitally deaf children receive implants in both ears. Vestibular concerns may arise if the patient is operated on in both ears simultaneously, or in the only vestibular functioning ear. Signs of damage to the saccule with loss of VEMP are common but seemingly with a limited correlation to vertigo, possibly due to transient disturbances (53) and central compensation (37, 41, 54). Colin et al. (4) prospectively tested vestibular function, using pre- and postoperative neuro-vestibular examination and clinical tests, and found no correlation between postoperative test results and postoperative vertigo. Occasionally, there was even improved balance following electric stimulation (4, 55, 56).

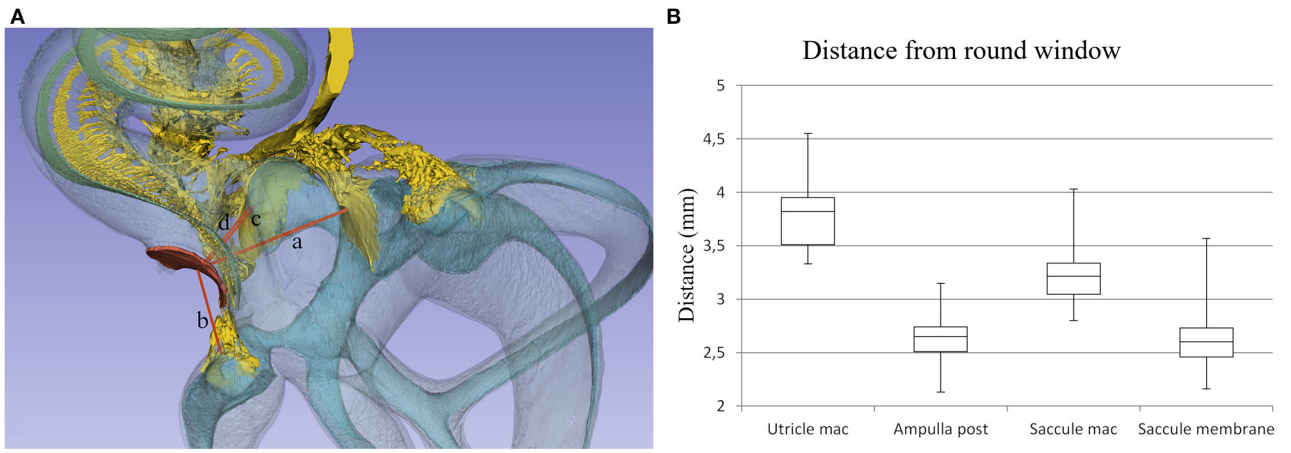

FIGURE 11 | (A) Distances from the (a) utricle macula, (b) posterior semicircular canal ampulla, (c) saccule macula, and (d) saccule membrane to the middle of the RW were assessed. **(B)** Box plot showing measurements in 22 temporal bones.

The present results using SR-PCI and micro-CT imaging three-dimensionally display the intriguing and difficult anatomy of the base of the cochlea and vestibular end-organs. This study may hopefully contribute to a better understanding of the spatial organization, thereby increasing surgical safety. Enhancement of surgical techniques, approaches, and design of CI electrodes may further lessen surgical trauma in the future.

DATA AVAILABILITY STATEMENT

The data supporting the conclusions of this article will be made available by the authors, upon request to the corresponding author.

ETHICS STATEMENT

The study was approved by Western University, London, Ontario, Canada, in accordance with the Anatomy Act of Ontario and Western's Committee for Cadaveric Use in Research (approval no. 06092020).

AUTHOR CONTRIBUTIONS

GR and JS performed micro-CT of human cadavers. HML and JS performed image processing and 3D visualization of scanned objects provided by SA, HL, SR, and JS. HR-A and NS-M planned the project. Microdissections with cochleostomies were provided by FA and HR-A. HR-A, SA, and HL analyzed the images and wrote the manuscript.

FUNDING

This study was supported by the Swedish Research Council [2017-03801], the Tysta Skolan Foundation, the Swedish Hearing Research Foundation (hrf), and generous private funds from Arne Sundström, Sweden. Part of the research described in this paper was performed at the Bio-Medical Imaging and Therapy (BMIT) facility at the Canadian Light Source, which is funded by the Canada Foundation for Innovation, the Natural Sciences and Engineering Research Council of Canada, the National Research Council Canada, the Canadian Institutes of Health Research, the Government of Saskatchewan, Western Economic Diversification Canada, and the University of Saskatchewan. The authors acknowledge support from the Natural Sciences and Engineering Research Council of Canada and the Province of Ontario. The project was supported by MED-EL Medical Electronics, Innsbruck, Austria under an agreement and contract with Uppsala University. The funder had no role in study design, data collection and analysis, decision to publish, or preparation of the manuscript.

ACKNOWLEDGMENTS

We gratefully thank MED-EL, Austria, and especially Susanne Braun and Carolyn Garnham from MED-EL Innsbruck. X-ray micro-CT scans were conducted by JS, and we wish to acknowledge the facilities and the scientific and technical assistance of Microscopy Australia at the Center for Microscopy, Characterization, & Analysis and the University of Western Australia, a facility funded by the university, state, and commonwealth governments.

SUPPLEMENTARY MATERIAL

The Supplementary Material for this article can be found online at: https://www.frontiersin.org/articles/10.3389/fneur.2021.663722/full#supplementary-material

REFERENCES

1. Dutt SN, Ray J, Hadjihannas E, Cooper H, Donaldson I, Proofs DW. Medical and surgical complications of the second 100 adult cochlear implant patients in Birmingham. *J Laryngol Otol.* (2005) 119:759–64. doi: 10.1258/002221505774481291
2. Enticott JC, Tari S, Koh SM, Dowell RC, O'Leary SJ. Cochlear implant and vestibular function. *Otol Neurotol.* (2006) 27:824–30. doi: 10.1097/01.mao.0000227903.47483.a6
3. Ibrahim I, Da Silva SD, Segal B, Zeitouni A. Effect of cochlear implant surgery on vestibular function: Meta-analysis study. *J Otolaryngol Head Neck Surg.* (2017) 46:44. doi: 10.1186/s40463-017-0224-0
4. Colin V, Bertholon P, Roy S, Karkas A. Impact of cochlear implantation on peripheral vestibular function in adults. *Eur Ann Otorhinolaryngol Head Neck Dis.* (2018) 135:417–20. doi: 10.1016/j.anorl.2018.10.007
5. Binnetoglu A, Demir B, Batman C. Surgical complications of cochlear implantation: a 25-year retrospective analysis of cases in a tertiary academic center. *Eur Arch Oto Rhino Laryngol.* (2020) 277:1917–23. doi: 10.1007/s00405-020-05916-w
6. Farinetti A, Ben Gharbia D, Mancini J, Roman S, Nicollas R, Triglia JM. Cochlear implant complications in 403 patients: comparative study of adults and children and review of the literature. *Eur Ann Otorhinolaryngol Head Neck Dis.* (2014) 131:177–82. doi: 10.1016/j.anorl.2013.05.005
7. Rah YC, Park JH, Park JH, Choi BY, Koo JW. Dizziness and vestibular function before and after cochlear implantation. *Eur Arch Oto Rhino Laryngol.* (2016) 273:3615–21. doi: 10.1007/s00405-016-3988-3
8. Tien HC, Linthicum FH. Histopathologic changes in the vestibule after cochlear implantation. *Otolaryngol Head Neck Surg.* (2002) 127:260–4. doi: 10.1067/mhn.2002.128555
9. Handzel O, Burgess BJ, Nadol JB. Histopathology of the peripheral vestibular system after cochlear implantation in the human. *Otol Neurotol.* (2006) 27:57–64. doi: 10.1097/01.mao.0000188658.36327.8f
10. Vogel U. New approach for 3D imaging and geometry modeling of the human inner ear. *ORL.* (1999) 61:259–67. doi: 10.1159/000027683
11. Müller B, Lareida A, Beckmann F, Diakov GM, Kral F, Schwarm F, et al. Anatomy of the murine and human cochlea visualized at the cellular level by synchrotron-radiation-based micro-computed tomography. In: *Developments in X-Ray Tomography V*. San Diego, CA: SPIE Optics + Photonics (2006). p. 631805. doi: 10.1117/12.680540
12. Lareida A, Beckmann F, Schrott-Fischer A, Glueckert R, Freysinger W, Muller B. High-resolution X-ray tomography of the human inner ear: synchrotron radiation-based study of nerve fibre bundles, membranes and ganglion cells. *J Microsc.* (2009) 234:95–102. doi: 10.1111/j.1365-2818.2009.03143.x
13. Koch RW, Elfarnawany M, Zhu N, Ladak HM, Agrawal SK. Evaluation of cochlear duct length computations using synchrotron radiation phase-contrast imaging. *Otol Neurotol.* (2017) 38:e92–9. doi: 10.1097/MAO.0000000000001410
14. Li H, Schart-Morén N, Rohani SA, Ladak HM, Rask-Andersen H, Agrawal S. Synchrotron radiation-based reconstruction of the human spiral ganglion: implications for cochlear implantation. *Ear Hear.* (2018) 41:173–81. doi: 10.1097/AUD.0000000000000738
15. Agrawal S, Schart-Morén N, Liu W, Ladak HM, Rask-Andersen H, Li H. The secondary spiral lamina and its relevance in cochlear implant surgery. *Ups J Med Sci.* (2018) 123:9–18. doi: 10.1080/03009734.2018.1443983
16. Elfarnawany M, Alam SR, Rohani SA, Zhu N, Agrawal SK, Ladak HM. Micro-CT versus synchrotron radiation phase contrast imaging of human cochlea. *J Microsc.* (2017) 265:349–57. doi: 10.1111/jmi.12507
17. Rau C, Robinson IK, Richter C-P. Visualizing soft tissue in the mammalian cochlea with coherent hard X-rays. *Microsc Res Tech.* (2006) 69:660–5. doi: 10.1002/jemt.20336
18. Iyer JS, Zhu N, Gasilov S, Ladak HM, Agrawal SK, Stankovic KM. Visualizing the 3D cytoarchitecture of the human cochlea in an intact temporal bone using synchrotron radiation phase contrast imaging. *Biomed Opt Express.* (2018) 9:3757. doi: 10.1364/BOE.9.003757
19. Enghag S, Strömbäck K, Li H, Rohani SA, Ladak HM, Rask-Andersen H, et al. Incus necrosis and blood supply: a micro-CT and synchrotron imaging study. *Otol Neurotol.* (2019) 40:E713–22. doi: 10.1097/MAO.0000000000002292
20. Rohani SA, Allen D, Gare B, Zhu N, Agrawal S, Ladak H. High-resolution imaging of the human incudostapedial joint using synchrotron-radiation phase-contrast imaging. *J Microsc.* (2020) 277:61–70. doi: 10.1111/jmi.12864
21. Anschuetz L, Demattè M, Pica A, Wimmer W, Caversaccio M, Bonnin A. Synchrotron radiation imaging revealing the sub-micron structure of the auditory ossicles. *Hear Res.* (2019) 383. doi: 10.1016/j.heares.2019.107806
22. Atturo F, Barbara M, Rask-Andersen H. On the anatomy of the "hook" region of the human cochlea and how it relates to cochlear implantation. *Audiol Neurotol.* (2014) 19:378–85. doi: 10.1159/000365585
23. Schart-Morén N, Agrawal SK, Ladak HM, Li H, Rask-Andersen H. Effects of various trajectories on tissue preservation in cochlear implant surgery: a micro-computed tomography and synchrotron radiation phase-contrast imaging study. *Ear Hear.* (2019) 40:393–400. doi: 10.1097/AUD.0000000000000624
24. Fedorov A, Beichel R, Kalpathy-Cramer J, Finet J, Fillion-Robin JC, Pujol S, et al. 3D Slicer as an image computing platform for the quantitative imaging network. *Magn Reson Imaging.* (2012) 30:1323–41. doi: 10.1016/j.mri.2012.05.001
25. Camilieri-Asch V, Shaw JA, Mehnert A, Yopak KE, Partridge JC, Collin SP. Dicect: A valuable technique to study the nervous system of fish. *eNeuro.* (2020) 7:1–23. doi: 10.1523/ENEURO.0076-20.2020
26. Culling CFA, Charles FA, Dunn WL. Developments in X-Ray tomography V. *In: SPIE Optics + Photonics. Vol. 6318.* Bonse U, (editor). San Diego, CA. (1974).
27. Wilbrand HF. Multidirectional tomography of the facial canal. *Acta Radiol Diagn.* (1975) 16:654–72. doi: 10.1177/028418517501600613
28. Rask-Andersen H, Stahle J, Wilbrand H. Human cochlear aqueduct and its accessory canals. *Ann Otol Rhinol Laryngol.* (1977) 86:1–16. doi: 10.1177/00034894770860S501
29. Atturo F, Barbara M, Rask-Andersen H. Is the human round window really round? An anatomic study with surgical implications. *Otol Neurotol.* (2014) 35:1354–60. doi: 10.1097/MAO.0000000000000332
30. Adunka OF, Radeloff A, Gstoettner WK, Pillsbury HC, Buchman CA. Scala tympani cochleostomy II: topography and histology. *Laryngoscope.* (2007) 117:2195–200. doi: 10.1097/MLG.0b013e3181453a53
31. Basura GJ, Adunka OF, Buchman CA. Scala tympani cochleostomy for cochlear implantation. *Oper Tech Otolaryngol Head Neck Surg.* (2010) 21:218–22. doi: 10.1016/j.otot.2010.08.001
32. Perlman HB. The saccule: observations on a differentiated reenforced area of the saccular wall in man. *Arch Otolaryngol Head Neck Surg.* (1940) 32:678–91. doi: 10.1001/archotol.1940.00660020683005
33. Limb CJ, Francis HF, Lustig LR, Niparko JK, Jammal H. Benign positional vertigo after cochlear implantation. *Otolaryngol Head Neck Surg.* (2005) 132:741–5. doi: 10.1016/j.otohns.2005.01.004
34. Yamane H, Takayama M, Sunami K, Sakamoto H, Mochizuki K, Inoue Y. Three-dimensional images of the reuniting duct using cone beam CT. *Acta Otolaryngol.* (2009) 129:493–6. doi: 10.1080/00016480802294393
35. Kusuma S, Liou S, Haynes DS. Disequilibrium after cochlear implantation caused by a perilymph fistula. *Laryngoscope.* (2005) 115:25–6. doi: 10.1097/01.mlg.0000150680.68355.cc
36. Fina M, Skinner M, Goebel JA, Piccirillo JF, Neely JG. Vestibular dysfunction after cochlear implantation. *Otol Neurotol.* (2003) 24:234–42. doi: 10.1097/00129492-200303000-00018
37. Basta D, Todt I, Goepel F, Ernst A. Loss of saccular function after cochlear implantation: the diagnostic impact of intracochlear electrically elicited vestibular evoked myogenic potentials. *Audiol Neurotol.* (2008) 13:187–92. doi: 10.1159/000113509
38. Todt I, Basta D, Ernst A. Does the surgical approach in cochlear implantation influence the occurrence of postoperative vertigo? *Otolaryngol Head Neck Surg.* (2008) 138:8–12. doi: 10.1016/j.otohns.2007.09.003
39. Jin Y, Nakamura M, Shinjo Y, Kaga K. Vestibular-evoked myogenic potentials in cochlear implant children. *Acta Otolaryngol.* (2006) 126:164–9. doi: 10.1080/00016480500312562
40. Meli A, Aud BM, Aud ST, Aud RG, Cristofari E. Vestibular function after cochlear implant surgery. *Cochlear Implants Int.* (2016) 17:151–7. doi: 10.1179/1754762815Y.0000000014

41. Licameli G, Zhou G, Kenna MA. Disturbance of vestibular function attributable to cochlear implantation in children. *Laryngoscope*. (2009) 119:740–5. doi: 10.1002/lary.20121
42. Sosna M, Tacikowska G, Pietrasik K, Skarzyński H, Lorens A, Skarzyński PH. Effect on vestibular function of cochlear implantation by partial deafness treatment–electro acoustic stimulation (PDT–EAS). *Eur Arch Oto Rhino Laryngol*. (2019) 276:1951–9. doi: 10.1007/s00405-019-05425-5
43. Rajan GP, Kontorinis G, Kuthubutheen J. The effects of insertion speed on inner ear function during cochlear implantation: a comparison study. *Audiol Neurotol*. (2012) 18:17–22. doi: 10.1159/000342821
44. Batuecas-Caletrio A, Klumpp M, Santacruz-Ruiz S, Gonzalez FB, Sánchez EG, Arriaga M. Vestibular function in cochlear implantation: correlating objectiveness and subjectiveness. *Laryngoscope*. (2015) 125:2371–5. doi: 10.1002/lary.25299
45. Veroul E, Sabban D, Blexmann L, Frachet B, Poncet-Wallet C, Mamelle E. Predictive factors of vertigo following cochlear implantation in adults. *Eur Arch Oto Rhino Laryngol*. (2020) 1:3. doi: 10.1007/s00405-020-06449-y
46. Nassif N, Balzanelli C, Redaelli De Zinis LO. Long-Term lateral semicircular canal function in children with cochlear implants: results of video head impulse test. *Eur J Investig Heal Psychol Educ*. (2021) 11:12–9. doi: 10.3390/ejihpe11010002
47. Hänsel T, Gauger U, Bernhard N, Behzadi N, Romo Ventura ME, Hofmann V, et al. Meta-analysis of subjective complaints of vertigo and vestibular tests after cochlear implantation. *Laryngoscope*. (2018) 128:2110–23. doi: 10.1002/lary.27071
48. Richter B, Aschendorff A, Lohnstein P, Husstedt H, Nagursky H, Laszig R. The nucleus contour electrode array: a radiological and histological study. *Laryngoscope*. (2001) 111:508–14. doi: 10.1097/00005537-200103000-00023
49. Rask-Andersen H, Liu W, Erixon E, Kinnefors A, Pfaller K, Schrott-Fischer A, et al. Human cochlea: anatomical characteristics and their relevance for cochlear implantation. *Anat Rec*. (2012) 295:1791–811. doi: 10.1002/ar.22599
50. Zeng J, Huang HM, Wang XQ, Zhong KB, Wu PN. [Assessment of the horizontal semicircular canal function after cochlear implantation by video head impulse test and caloric test]. *Lin Chung Er Bi Yan Hou Tou Jing Wai Ke Za Zhi*. (2018) 32:86–90. doi: 10.13201/j.issn.1001-1781.2018.02.002
51. Dagkiran M, Tuncer U, Surmelioglu O, Tarkan O, Ozdemir S, Cetik F, et al. How does cochlear implantation affect five vestibular end-organ functions and dizziness? *Auris Nasus Larynx*. (2019) 46:178–85. doi: 10.1016/j.anl.2018.07.004
52. Nassif N, Balzanelli C, Redaelli de Zinis LO. Preliminary results of video head Impulse TESTING (vHIT) in children with cochlear implants. *Int J Pediatr Otorhinolaryngol*. (2016) 88:30–3. doi: 10.1016/j.ijporl.2016.06.034
53. Jacot E, Van Den Abbeele T, Debre HR, Wiener-Vacher SR. Vestibular impairments pre- and post-cochlear implant in children. *Int J Pediatr Otorhinolaryngol*. (2009) 73:209–17. doi: 10.1016/j.ijporl.2008.10.024
54. Ajalloueyan M, Saeedi M, Sadeghi M, Zamiri Abdollahi F. The effects of cochlear implantation on vestibular function in 1–4 years old children. *Int J Pediatr Otorhinolaryngol*. (2017) 94:100–3. doi: 10.1016/j.ijporl.2017.01.019
55. Buchman CA, Joy J, Hodges A, Telischi FF, Balkany TJ. Vestibular effects of cochlear implantation. *Laryngoscope*. (2004) 114:1–22. doi: 10.1097/00005537-200410001-00001
56. Krause E, Louza JPR, Wechtenbruch J, Hempel JM, Rader T, Grkov R. Incidence and quality of vertigo symptoms after cochlear implantation. *J Laryngol Otol*. (2009) 123:278–82. doi: 10.1017/S00222151080 0296X

Conflict of Interest: MED-EL Medical Electronics, R&D, GmbH, and Innsbruck, Austria provided salary support for one research group member (HL) in accordance with the contract agreement with Uppsala University, Sweden 2018.

The remaining authors declare that the research was conducted in the absence of any commercial or financial relationships that could be construed as a potential conflict of interest.